

Exploring dynamical quantum phase transition from pure states to mixed states through generalized Su-Schrieffer-Heeger models

Kaiyuan Cao and Jian Wang*

College of Physics Science and Technology, Yangzhou University, Yangzhou 225002, China

(Dated: January 14, 2025)

We investigate dynamic quantum phase transitions (DQPTs) in both pure and mixed states within the framework of the generalized SSH model, specifically analyzing the SSH-3 and SSH-4 models, which exhibit different symmetries. We find that the SSH-3 model, characterized by a chiral-like point symmetry rather than true chiral symmetry, supports robust localized edge states associated with its topological properties. Our results show that DQPTs for pure states occur following a quench that crosses the topological transition, even with an open energy band gap. For mixed states, DQPT behavior is consistent at low temperatures, but significant changes are observed at high temperatures, resulting in the emergence of multiple critical times. In contrast, the SSH-4 model, which possesses chiral symmetry, allows for the analysis of two distinct energy spectrum configurations. We conclude that the occurrence of DQPTs for pure states in the SSH-4 model necessitates a quench from an initial state without a band gap while crossing the critical point of the topological transition, whereas DQPTs are absent for mixed states at elevated temperatures.

I. INTRODUCTION

Recent experimental investigations on ultra-cold atoms confined in optical lattices [1, 2] have significantly advanced the exploration of non-equilibrium dynamics in isolated quantum systems [3]. A primary focus within this field is the temporal evolution of a quantum system following a sudden global quench, which can be readily performed in experiments and studied theoretically [4]. In these scenarios, the Loschmidt echo, indicating the overlap between the pre- and post-quench Hamiltonian eigenstates, plays a pivotal role [5]. The formal parallelism between the Loschmidt amplitude and the canonical partition function of an equilibrium system has led to the concept of dynamical quantum phase transitions (DQPTs), aiding in the comprehension of phase and phase transition concepts in non-equilibrium settings [6–8].

The concept of dynamical quantum phase transitions (DQPTs) elucidates the critical behaviors of the Loschmidt echo, $\mathcal{L}(t) = |\mathcal{G}(t)|^2$, in the non-equilibrium evolution of quantum systems. The Loschmidt amplitude, $\mathcal{G}(t)$, quantifying the overlap between evolving and initial states, is expressed as $\mathcal{G}(t) = \langle \psi_0 | e^{-iHt} | \psi_0 \rangle$. To reveal DQPTs, the dynamical free energy density as the rate function of the Loschmidt echo in the thermodynamic limit, $\lambda(t) = -\lim_{N \rightarrow +\infty} \frac{1}{N} \ln [\mathcal{L}(t)]$, or its time derivative, exhibits cusp-like singularities at critical times. DQPTs have been extensively analyzed in various quantum systems, encompassing XY chains [9–12], Kitaev honeycomb models [13], non-integrable models [14–18], systems with long-range interactions [19–25], quantum Potts models [26], non-Hermitian systems [27–30], Bose-Einstein condensates [31], periodically driven systems [32–39], mixed states [40–49], among others. Experimental validations of DQPTs have been achieved

through trapped ions simulations [50–53], nuclear magnetic resonance quantum simulators [54], quantum walks of photons [55, 56], and spinor condensate simulations [57]. Moreover, an alternative definition of DQPTs examines the late-time behavior of order parameters [58–62], revealing two types of DQPTs in the long-range quantum Ising chain [24].

Recent advancements have unveiled that DQPTs can shed light on the topological aspects of real-time quench dynamics [63]. In this regard, a bulk topological quantum number, derived from the momentum space winding number of the Pancharatnam geometric phase, has been introduced to encapsulate these topological characteristics, known as the dynamic topological order parameter (DTOP). The DQPTs involving topological properties have received some attention, especially in band models [64–66]. However, whether existing conclusions can be generalized to quantum band systems with certain special symmetries remains an open question. For example, in the case of SSH-3, despite having robust localized edge states, it lacks the chiral symmetry and topological invariants characteristic of the SSH model [67]. Therefore, in this paper, we focus on the influence of the symmetry of band models on the properties of dynamical quantum phase transitions. To this end, we study the extended SSH model, primarily analyzing the dynamical quantum phase transition behavior of two typical models after quenching. We also discuss the impact of finite temperatures on the dynamical behavior.

The paper is organized as follows: In Sec. II, we introduce the generalized SSH model and derive the time-dependent state of the system after a quantum quench. In Secs. III and IV, we investigate the behavior of DQPTs for both pure and mixed states in the SSH-3 model. In Sec. V, we study the property of the DQPT in the SSH-4 model. We conclude in Sec. VI

* wangjian@yzu.edu.cn

II. MODEL

We explore a generalized version of the SSH model, referred to as the SSH-m model. The Hamiltonian for this model is expressed as follows:

$$H = - \sum_{n=1}^N (t_1 |n, A\rangle \langle n, B| + \cdots + t_{m-1} |n, M-1\rangle \langle n, M|) - \sum_{n=1}^N t_m |n, M\rangle \langle n+1, A| + H.c., \quad (1)$$

where t_1, \dots, t_{m-1} represent intracell couplings, and t_m denotes the intercell coupling. In contrast to the SSH model, the generalized SSH-m model reveals richer variety of topological phase transitions [67, 68]. In the Hamiltonian (1), we have imposed the periodic boundary condition. Consequently, the Bloch Hamiltonian is obtained by

$$H_k = \begin{pmatrix} 0 & t_1 & 0 & \cdots & t_m e^{-ik} \\ t_1 & \ddots & \ddots & \ddots & \vdots \\ 0 & \ddots & 0 & \ddots & 0 \\ \vdots & \ddots & \ddots & \ddots & t_{m-1} \\ t_m e^{ik} & \cdots & 0 & t_{m-1} & 0 \end{pmatrix}, \quad (2)$$

where k is the lattice momentum.

Firstly we consider a quantum quench starting from t_3^i to t_3^f . The initial state is prepared at the pure state $|u_{k\mu}^i\rangle$, which satisfying

$$H_k(t_1^i) |u_{k\mu}^f\rangle = \varepsilon_{k\mu}^i |u_{k\mu}^i\rangle, \mu = 1, \dots, m. \quad (3)$$

The time-evolved state following the quench is then given by

$$|\psi_k(t)\rangle = e^{-iH_k(t_1^f)t} |u_{k\mu}^i\rangle. \quad (4)$$

To calculate Eq. (4), we can write the initial state as a linear superposition of eigenstates of post-quench Hamiltonian, which yields

$$|u_{k\mu}^i\rangle = \sum_{\nu=1}^m p_{k\nu} |u_{k\nu}^f\rangle, \quad p_{k\nu} = \langle u_{k\nu}^f | u_{k\mu}^i \rangle. \quad (5)$$

Substituting Eq. (5) into (4), we obtain the time-evolved state as

$$|\psi_k(t)\rangle = \sum_{\nu=1}^m p_{k\nu} e^{-i\varepsilon_{k\nu}^f t} |u_{k\nu}^f\rangle. \quad (6)$$

We thus obtain the Loschmidt amplitude $\mathcal{G}(t) = \prod_k \mathcal{G}_k(t)$ immediately with

$$\mathcal{G}_k(t) = \langle u_{k\mu}^i | \psi_k(t) \rangle = \sum_{\nu=1}^m |p_{k\nu}|^2 e^{-i\varepsilon_{k\nu}^f t}. \quad (7)$$

It is convenient to express the Loschmidt amplitude $\mathcal{G}_k(t)$ as

$$\mathcal{G}_k(t) = r_k(t) e^{i\phi_k(t)} \quad (8)$$

in the polar coordinate, so that the Loschmidt echo can thus be obtained by

$$\mathcal{L}(t) = \prod_k \mathcal{L}_k(t), \quad \mathcal{L}_k(t) = r_k^2(t). \quad (9)$$

In the thermodynamic limit, the DQPTs are identified by the cusp-like singularities of the dynamical free energy density, which is defined as the rate function of the Loschmidt echo:

$$\lambda(t) = - \lim_{N \rightarrow \infty} \frac{1}{N} \ln [\mathcal{L}(t)] = - \int_{-\pi}^{\pi} \frac{dk}{2\pi} \ln r_k^2(t). \quad (10)$$

Since $r_k(t)$ is well-defined, the singularities of the rate function $\lambda(t)$ occur only for $r_k(t) = 0$, which is known as the Fisher zeros of the Loschmidt amplitude. At the Fisher zeros of $\mathcal{G}_k(t)$, the associate phase $\phi_k(t)$ is ill-defined, which induces the DTOP. According to Berry's theory, the total phase $\phi_k(t)$ consists of a geometric phase $\phi_k^G(t)$ and a dynamical phase $\phi_k^{dyn}(t)$, in which the latter is contributed from the accumulation of the energy. In our model, the dynamical phase for the pure state can be obtained by

$$\phi_k^{dyn}(t) = - \sum_{\nu=1}^m |p_{k\nu}|^2 \varepsilon_{k\nu}^f t. \quad (11)$$

As a result, the Pancharatnam geometric phase following the quench is given by

$$\phi_k^G(t) = \text{Arg}[\mathcal{G}_k(t)] - \phi_k^{dyn}(t). \quad (12)$$

In contrast, when considering the dynamics at finite temperature, the initial state is prepared as the thermal state described by a full-ranked density matrix ρ_0 . The density matrix at time t after the quench is given by $\rho(t) = e^{-iH(t)} \rho_0 e^{iHt}$. Hence, a generalization of the Loschmidt amplitude to general density matrices we consider is defined as [40, 41]

$$\mathbb{G}(t) = \text{Tr}[\rho_0 U(t)] = \prod_k g L_k(t) = \prod_k \text{Tr}[\rho_{0k} U_k(t)]. \quad (13)$$

It is important to emphasize that the generalized Loschmidt amplitude proposed here is not limited by the parallel transport condition [42, 69–71]. In our model, the initial density matrices for every k take the form

$$\rho_{0k} = \sum_{\mu=1}^m f_{k\mu} |u_{k\mu}^i\rangle \langle u_{k\mu}^i|, \quad (14)$$

where the probabilities $f_{k\mu} \in (0, 1]$ of the electron occupying $|u_{k\mu}^i\rangle$ parameterize the thermal state

$$f_{k\mu} = \frac{e^{-\beta \varepsilon_{k\mu}^i}}{\sum_{\mu=1}^m e^{-\beta \varepsilon_{k\mu}^i}}. \quad (15)$$

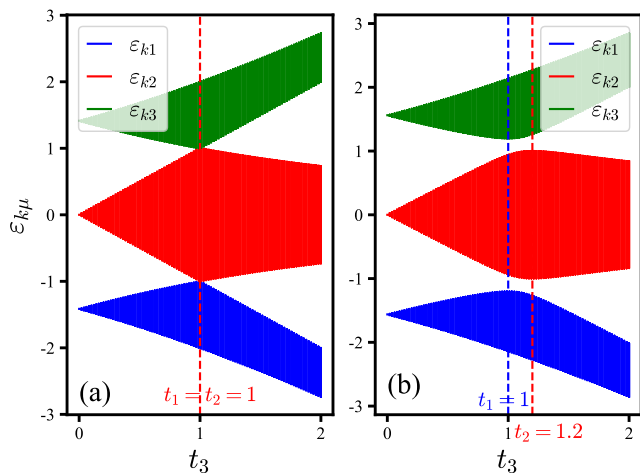


FIG. 1. The energy spectra as functions of t_3 in the SSH-3 models for (a) with $t_1 = t_2 = 1$, and (b) with $t_1 = 1, t_2 = 1.2$. In (a), the gaps of the energy spectra vanish at $t_3 = t_1 = t_2 = 1$.

Here, $\beta = 1/T$ is the inverse temperature. For simplicity, we set $c = \hbar = k_b = 1$ in our paper. Substituting Eq. (14) into Eq. (13), we immediately obtain the generalized Loschmidt overlap amplitude by

$$\mathbb{G}(t) = \sum_{\mu=1}^m f_{k\mu} \sum_{\nu=1}^m |p_{k\nu}|^2 e^{-i\varepsilon_{k\nu}^f t}. \quad (16)$$

For a pure initial state $|u_{k\mu}^i\rangle$, i.e. $f_{k\mu} = 1$, Eq. (16) returns back to Eq. (7).

Similarly, we can also express the generalized Loschmidt amplitude in the polar coordinate, i.e. $\mathbb{G}_k(t) = R_k(t)e^{i[\Phi_k^{dyn}(t) + \Phi_k^G(t)]}$, where the dynamical phase for the mixed state is defined as

$$\Phi_k^{dyn}(t) = - \int_0^t \text{Tr}[\rho(s)H_k(t_1^f)] ds \quad (17)$$

Selecting the eigenstates of the post-quench Hamiltonian as a set of basis, i.e. $\{|u_{k\nu}^f\rangle\}, \nu = 1, \dots, m$, we obtain

$$\begin{aligned} \Phi_k^{dyn}(t) &= - \int_0^t \sum_{\nu=1}^m \langle u_{k\nu}^f | \rho_k(s) H_k(t_1^f) | u_{k\nu}^f \rangle ds \\ &= - \sum_{\mu=1}^m f_{k\mu} \sum_{\nu=1}^m |p_{k\nu}|^2 \varepsilon_{k\nu}^f t. \end{aligned} \quad (18)$$

Since two-band systems (i.e. SSH-2 model in our paper) have been widely studied, we consider the main results of the SSH-3 and SSH-4 models in the following.

III. DQPTs FOR PURE STATES IN SSH-3 MODEL

In this section, we consider a generalization of the SSH model hosting three lattice sites in a unit cell. Notably,

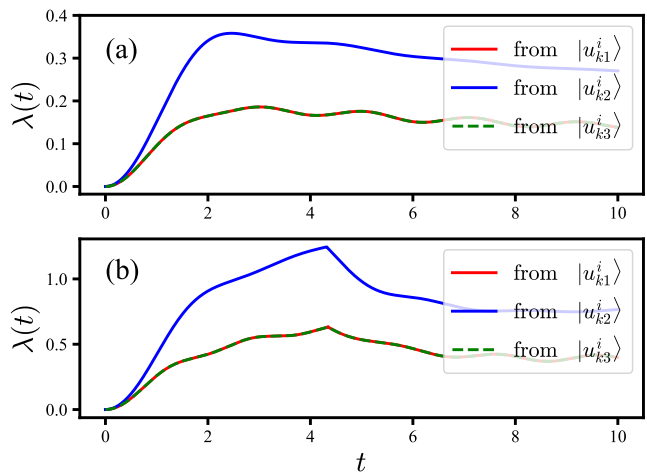


FIG. 2. (a) The rate functions in the SSH-3 models with the gap-closing point [see Fig. 1 (a)] for the quenches from different initial states, where the quenches are from $t_3^i = 0.2$ to $t_3^f = 0.8$. (b) The rate functions for different initial states, in which the quenches are from $t_3^i = 0.2$ to $t_3^f = 1.1$.

for the 1D SSH-3 model, the spectrum of the bulk Hamiltonian is not symmetric concerning zero [67], implying that the system does not possess chiral symmetry. The winding number is also not well-defined for the SSH-3 model [72]. However, the bulk Hamiltonian exhibits an additional interesting symmetry called point chirality, i.e. $\Gamma_k H_k \Gamma_k^\dagger = -H_{\pi-k}$ with $\Gamma_k = \text{diag}(1, -1, 1)$. In Fig. 1, we show the energy spectra of the bulk Hamiltonians for varying t_3 with fixed inner-cell hopping parameters t_1 and t_2 . The Hamiltonian exhibits the gap closing only when $t_1 = t_2 = t_3$, which exactly corresponds to the case of the SSH model.

A. DQPTs for the case with closing gap

Firstly, we examine the dynamics of DQPT in the scenario where a gap closing point is present, as shown in the energy spectra in Fig. 1 (a). According to numerous studies, the collapse of a band gap is crucial in the theory of DQPTs. When the gap reopens, the system undergoes a DQPT. In Figs. 2(a) and (b), we present the typical rate function results for quenches that do not cross the gap closing point and for those that do, respectively. It is evident that a DQPT occurs only for quenches that cross the gap closing point. Additionally, we observe that point chiral symmetry causes the rate functions to initially be identical for both the lowest ($|u_{k1}^i\rangle$) and the highest ($|u_{k3}^i\rangle$) bands.

Furthermore, we would like more information by investigating the Pancharatnam geometric phase. As shown in Fig. 3 (a) to (c), we display the Pancharatnam geometric phases in the (k, t) plane for the quenches from different initial bands respectively, where the quench is

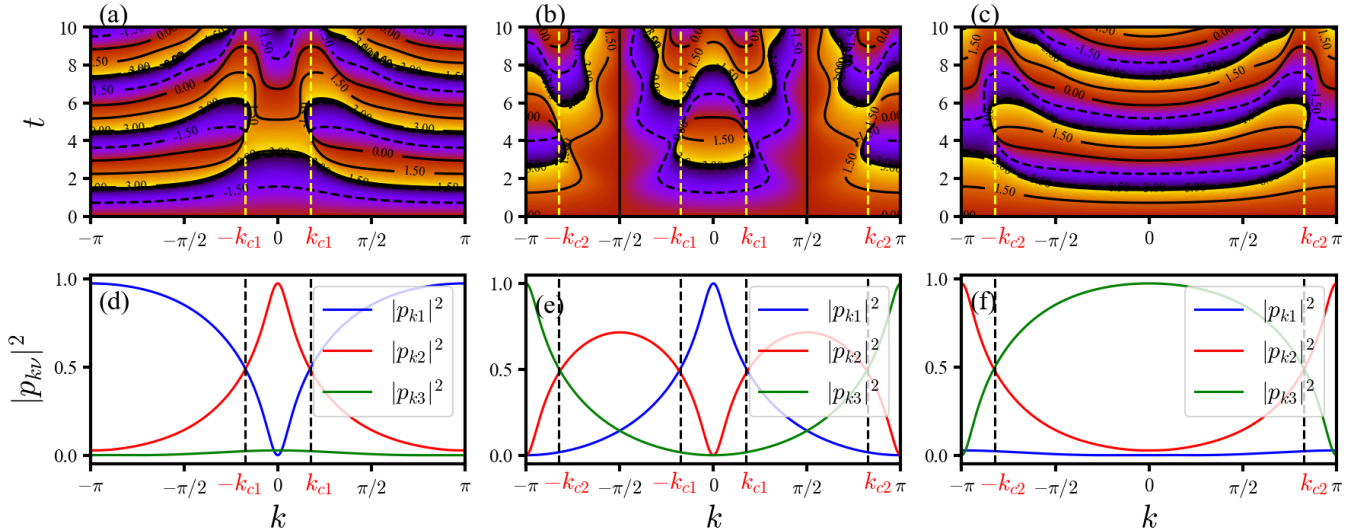


FIG. 3. (a)-(c) The Pancharatnam geometric phases in the SSH-3 model with the gap-closing point [see Fig. 1 (a)] for different initial states ($|u_{k1}^i\rangle$, $|u_{k2}^i\rangle$, and $|u_{k3}^i\rangle$) are shown in momentum-time space, respectively. The dynamical phase vortices marked by the white circles exhibit the critical wave vectors and times. (d)-(f) The corresponding transition probabilities $|p_{k\nu}|^2$ for different initial states. The quench paths are from $t_3^i = 0.2$ to $t_3^f = 1.1$ with fixed $t_1 = t_2 = 1$.

from $t_3^i = 0.2$ to $t_3^f = 1.2$. It is observed that the dynamical vortices as the signal of DQPTs show at the critical wave vectors k_c and the critical times t_c . Interestingly, we notice that for quenches from the initial states $|u_{k1}^i\rangle$ and $|u_{k3}^i\rangle$, there is one critical wave vector for $k > 0$, but two critical wave vectors ($k > 0$) for the quench from $|u_{k2}^i\rangle$. These critical wave vectors satisfy the following relation:

$$k_{c1} + k_{c2} = \pi, \quad (19)$$

as we specifically marked in the Fig. 3.

In two-band systems, the critical wave vector k_c is closely related to the equal transition probabilities, i.e. $|p_{k1}|^2 = |p_{k2}|^2 = 1/2$. Our three-level model also has a similar relation involving two energy bands whose gap collapses at the critical case $t_1 = t_2 = t_3$. In Fig. 3 (d) to (f), we show the transition probabilities as functions of k for quenches corresponding to that for Fig. 3 (a) to (c), respectively. It is observed that for the quench from $|u_{k1}^i\rangle$, the critical wave vector k_{c1} can be obtained by solving

$$|p_{k1}|^2 = |p_{k2}|^2. \quad (20)$$

Additionally, the wave vector k_{c2} is obtain by

$$|p_{k2}|^2 = |p_{k3}|^2 \quad (21)$$

for quenches from $|u_{k2}^i\rangle$ or $|u_{k3}^i\rangle$.

B. Surprising DQPTs for the case with gap

Now, we consider the DQPT where the gap of energy bands is always present, as shown in Fig. 1 (b). In previous studies, it was generally believed that an energy

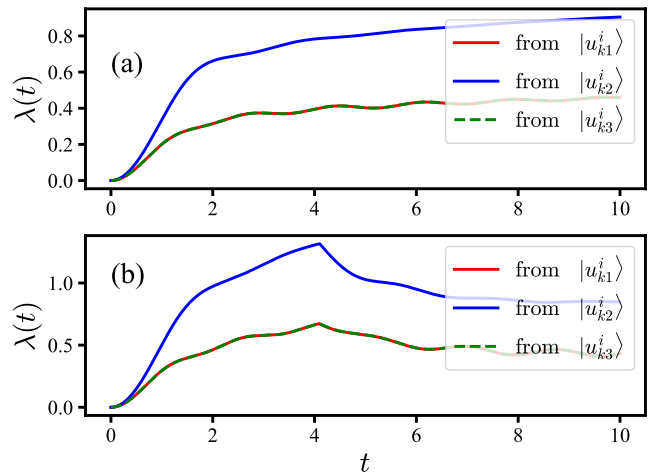


FIG. 4. (a) The rate functions in the SSH-3 models with the gap all the time [see Fig. 1 (b)] for the quenches from different initial states, where the quenches are from $t_3^i = 0.2$ to $t_3^f = 1.1$. (b) The rate functions for different initial states, in which the quenches are from $t_3^i = 0.2$ to $t_3^f = 1.3$.

gap would not lead to a DQPT in the system. However, in the SSH-3 model, the situation is different. By fixing $t_1 = 1$ and $t_2 = 1.2$, we show the rate function for the quench from $t_3^i = 0.2$ to $t_3^f = 1.1$ in Fig. 4 (a). Compared with that in Fig. 2 (b), the smooth rate function reveals that the presence of an energy gap may result in the disappearance of DQPTs. However, when $t_3^f = 1.3$, the rate function shows a cusp-like singularity point [see Fig. 4 (b)]. This implies that there is a critical value t_{3c} ,

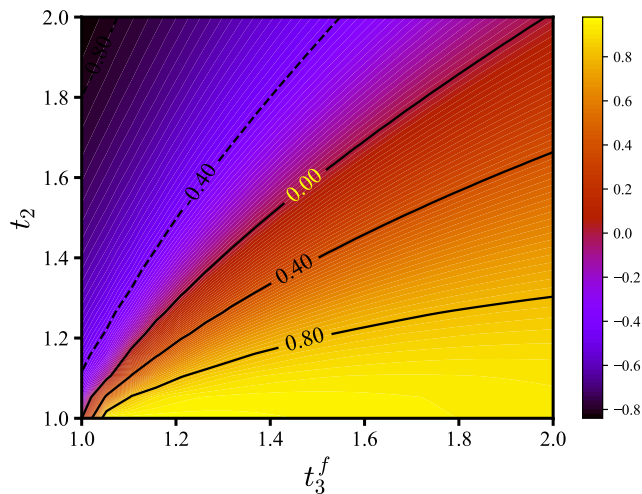


FIG. 5. The value of $\max(|p_{k2}|^2) - \min(|p_{k1}|^2)$ in the SSH-3 model with the gap all the time [see Fig. 1 (b)] for quenches from the initial state $|u_{k1}^i\rangle$. Here, we fix the parameter $t_1 = 1$ and the initial parameter $t_3^i = 0.2$ to see the critical lines, i.e. $\max(|p_{k2}|^2) - \min(|p_{k1}|^2) = 0$, for different t_2 and t_3^f .

and when the quench crosses this critical value ($t_3^f > t_{3c}$), a DQPT will occur even though the gap is still there.

To determine the critical value, we can utilize condition (20) [or (21)]. According to the results in 3 (d) to (f), we know that the condition ensuring (20) is satisfied is given by

$$\min(|p_{k1}|^2) < \max(|p_{k2}|^2). \quad (22)$$

Clearly, when the post-quench parameter is set at the critical point, we have $\min(|p_{k1}|^2) = \max(|p_{k2}|^2)$. In Fig. 5, we display the value of $\max(|p_{k2}|^2) - \min(|p_{k1}|^2)$ for quench from the lowest band $|u_{k1}^i\rangle$ varies as t_2 and t_3^f with fixed $t_1 = 1$ and $t_3^i = 0.2$, where the critical value t_{3c} is denoted by $\max(|p_{k2}|^2) - \min(|p_{k1}|^2) = 0$. It can be observed that the critical value t_{3c} is closely related to t_2 , although their relationship is not linear. To be precise, the critical value is always slightly less than t_2 except $t_2 = 1$. When $t_2 = 1$, the system returns to the scenario of the vanishing energy gap described in Sec. III A. This result once again verifies the conclusion of the previous section, namely that quenching through the topological transition leads to a DQPT. In fact, the results of this section can also be understood as the same conclusion: when $t_1 \neq t_2$ ($t_2 > t_1$), the SSH-3 model has a hidden topological transition point at $t_3 = t_2$. A change in the number of edge states under open boundary conditions characterizes this topological transition point.

IV. DQPT FOR MIXED STATES IN SSH-3 MODEL

In this section, we investigate the effect of the finite temperature on the DQPT, in which the general-

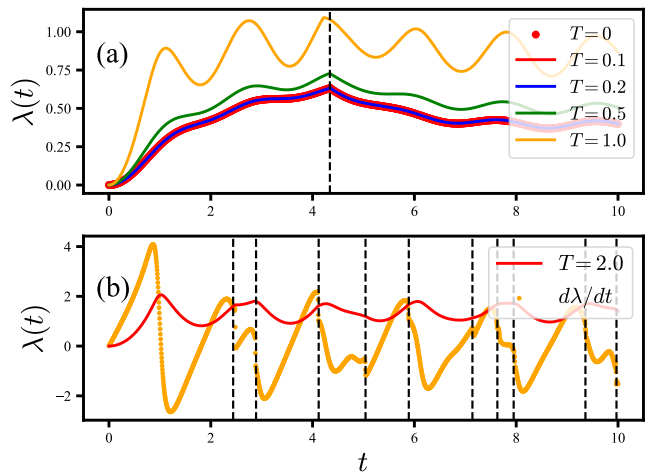


FIG. 6. (a) The rate functions in the SSH-3 model for mixed states at different temperatures ($T = 1/\beta$), where the quenches are all from $t_3^i = 0.2$ to $t_3^f = 1.1$, with fixed $t_1 = t_2 = 1$. The red-dot line denotes the rate function for the initial state $|u_{k1}^i\rangle$. (b) The rate function and its derivative $d\lambda/dt$ for the initial state at high $T = 2.0$. The later is used to highlight the critical times more clearly. The dashed lines mark the critical times.

ized Loschmidt amplitude for mixed states is calculated. Fig. 7 shows the rate functions in the SSH-3 model for initial states at different temperatures. It can be observed that at very low temperatures, i.e. $T = 0.1$ and $T = 0.2$, the rate function almost coincides with the result of that starting from the initial pure states $|u_{k1}^i\rangle$. This indicates that the behavior of the DQPT is not affected at low temperatures. As the temperature increases, the critical time will gradually deviate from the critical time at pure states and lower temperatures. Especially, at $T = 0.5$, the numerical values of the rate function change but the critical time still equals that at lower temperatures. However, when the temperature is very high, the nature of DQPTs will undergo significant changes, to the extent that we observe a large number of critical times emerging in the system through the first derivative $d\lambda/dt$ of the rate function. In addition, we also observe the same behavior of DQPTs from the Pancharatnam geometric phase (see Fig. 7). In particular, at high temperature, i.e. $T = 2.0$, the Pancharatnam geometric phase can be seen to exhibit many dynamical vortices emerging in the $(k - t)$ plane.

The behavior of the DQPT for mixed states at finite temperatures can be explained based on the properties of that for pure states. At lower temperatures, the probabilities $f_{k\mu}$ of the thermal states satisfy

$$f_{k1} \gg f_{k2} > f_{k3}, \quad (23)$$

thus the generalized Loschmidt amplitude is approximately equal to the case starting from the lowest energy band in the pure state. As the temperature increases,

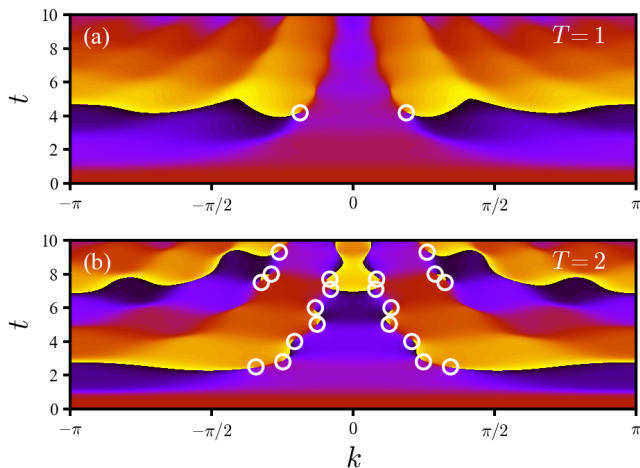


FIG. 7. The Pancharatnam geometric phases in the SSH-3 model for initial states at different temperatures, (a) $T = 1$, and (b) $T = 2$. The quench paths are from $t_3^i = 0.2$ to $t_3^f = 1.1$, with fixed $t_1 = t_2 = 1$. The dynamical vortices are highlighted in white.

the probabilities $f_{k\mu}$ of the thermal states change to

$$f_{k1} > f_{k2} \gg f_{k3}, \quad (24)$$

so that the generalized Loschmidt amplitude is approximately equal to the cases only mixing the quench from pure states $|u_{k1}^i\rangle$ and $|u_{k2}^i\rangle$. According to Fig. 3, we know that the cases of quenches from initial states $|u_{k1}^i\rangle$ and $|u_{k2}^i\rangle$ have the common critical wave vectors k_{c1} and $-k_{c1}$. In this case, the critical times for mixed states still do not change or just deviate slightly from that at lower temperatures. However, at high temperatures, due to the contribution of that from the highest band $|u_{k3}^i\rangle$ no longer being negligible, and considering the cases of quenches from the initial pure states $|u_{k2}^i\rangle$ and $|u_{k3}^i\rangle$ have another common critical time $k_{c2}(-k_{c2})$, which differs from k_{c1} , the generalized Loschmidt amplitude $\mathbb{G}(t)$ will not have the zeros at k_{c1} and k_{c2} . Consequently, the behavior of the DQPT at high temperatures is significantly changed.

V. DQPTS IN SSH-4 MODEL

As another typical example, we discuss the dynamic behavior in the SSH-4 model in this section. Unlike the SSH-3 model, the Bloch Hamiltonian of the SSH-4 model satisfies the chiral symmetry, leading to the energy spectrum of the SSH-4 being symmetric about the transverse axis ($\varepsilon_k = 0$) for a specific set of parameters, i.e.

$$\varepsilon_{k1} = -\varepsilon_{k4}, \quad \varepsilon_{k2} = -\varepsilon_{k3}. \quad (25)$$

By calculating the energy spectra under different parameters, we have identified three typical energy spectrum configurations in the SSH-4 model, one of which resembles the energy spectra of the period-two Kitaev chain,

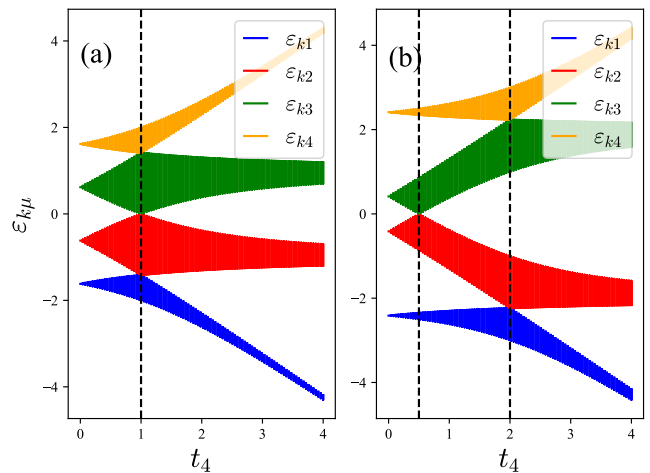


FIG. 8. The energy spectra as functions of t_4 in the SSH-4 models for (a) with $t_1 = t_2 = t_3 = 1$, and for (b) with $t_1 = t_3 = 1$ and $t_2 = 2$.

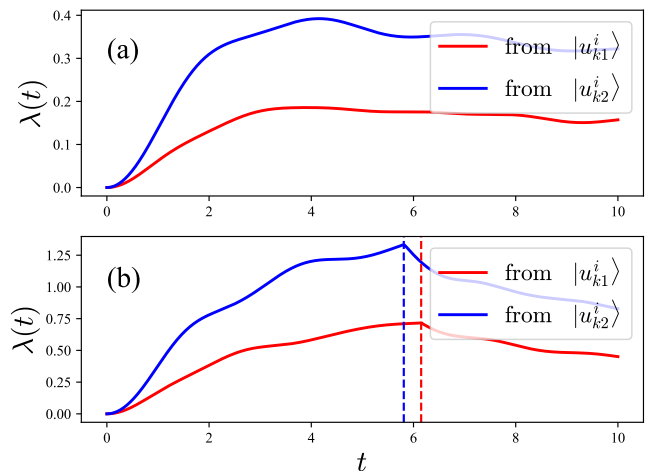


FIG. 9. The rate functions in the SSH-4 model with the energy spectrum configuration corresponding to Fig. 8 (a) for the quenches from different initial states. The quench path in (a) is from $t_4^i = 0.2$ to $t_4^f = 0.8$, and in (b) is from $t_4^i = 0.2$ to $t_4^f = 1.2$.

as discussed in the Ref. [66]. In this article, we will discuss two other cases different from the period-two Kitaev chains, with the shapes of their energy spectra shown in Fig. 8.

From Fig. 8 (a), it can be seen the system with parameters $t_1 = t_2 = t_3$ has a gap-closing point at $t_{4c} = 1$. In contrast, as shown in Fig. 8 (b), the system with parameters $t_1 = t_3 = 1$ and $t_2 = 2$ has two gap-closing points at $t_{4c} = 0.5$ and $t_{4c} = 2$. These critical points that collapse the energy bands will result in the topological transitions in the system, which are characterized by the change in the number of edge modes [68]. It is evident that based on previous experience, we can speculate that in the SSH-4 model, the behavior of the DQPT af-

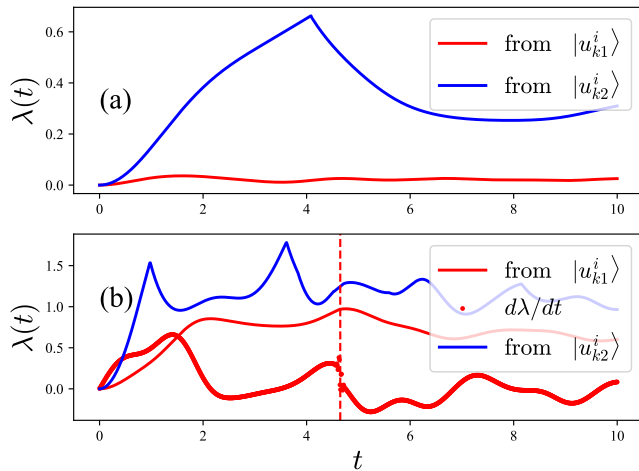


FIG. 10. The rate functions in the SSH-4 model with the energy spectrum configuration corresponding to Fig. 8 (b) for the quenches from different initial states. The quench path in (a) crossing the first critical point $t_{4c} = 0.5$ is from $t_4^i = 0.2$ to $t_4^f = 0.8$, and in (b) also crossing the second critical point $t_{4c} = 2$ is from $t_4^i = 0.2$ to $t_4^f = 2.2$. The first deviation $d\lambda/dt$ of the rate function for the quench from the initial state $|u_{k1}^i\rangle$ is shown to see the critical time more clearly.

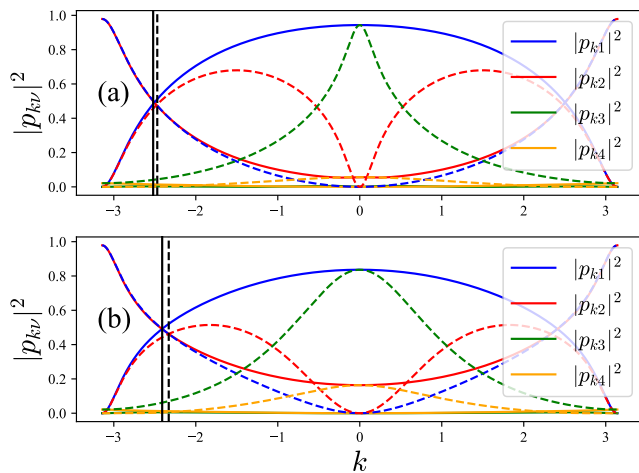


FIG. 11. The transition probabilities $|p_{k\nu}|^2$ in the SSH-4 model. The results in (a) correspond to the quench path of Fig. 9 (b), and in (b) correspond to that of Fig. 10 (b). The solid lines denote the results of the quench from the initial state $|u_{k1}^i\rangle$, and the dashed lines denote the results of the quench from the initial state $|u_{k2}^i\rangle$.

ter a quench will depend on whether the quench passes through these critical points.

Figs. 9 and 10 present the rate functions obtained from quenches starting from different initial states in the SSH-4 model with two different energy spectrum configurations, respectively. It is worth noting that due to the chiral symmetry resulting in a symmetric relationship between energy spectra, as shown in Eq. (25), the rate

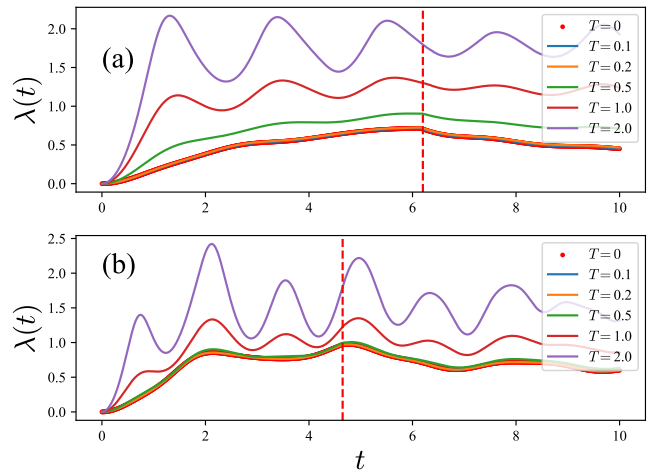


FIG. 12. The rate functions in the SSH-4 model for mixed states at different temperatures. The results in (a) correspond to the quench path of Fig. 9 (b), and in (b) correspond to that of Fig. 10 (b). The red-dot line denotes the rate function for the initial state $|u_{k1}^i\rangle$.

functions for quenches from the initial bands $|u_{k3}^i\rangle$ and $|u_{k4}^i\rangle$ are identical to those from $|u_{k2}^i\rangle$ and $|u_{k1}^i\rangle$. Therefore, it is sufficient to show the results of the quenches from $|u_{k1}^i\rangle$ and $|u_{k2}^i\rangle$ in the SSH-4 model. By comparing these results, we can verify our previous speculation that the system will only undergo a DQPT when the quench passes through the critical points. Interestingly, since the critical point at $t_{4c} = 0.5$ corresponds to the closing of the energy gaps between bands ε_{k2} and ε_{k3} , the quench from the initial state $|u_{k1}^i\rangle$ does not induce a DQPT even if it only crosses the critical point $t_{4c} = 0.5$ [see Fig. 10 (a)].

Some details in the results are also worth noting. In the SSH-3 model, we observe that the critical times obtained from quenches starting from different initial states are the same. However, in the SSH-4 model, the situation is different. From Figs. 9 (b) and 10 (b), it can be seen that the critical times of the rate functions for the quenches starting from $|u_{k1}^i\rangle$ and $|u_{k2}^i\rangle$ are not equal. This difference is also reflected in the deviation of the critical wave vectors [see Fig. 1 (a) and (b)]. While these details may seem less important in the context of pure-state DQPTs, they will significantly alter the behavior of mixed-state DQPTs.

To investigate the influence of finite temperature on DQPTs, we present in Fig. 12 the rate functions obtained from mixed states at different initial temperatures. It can be observed that when the temperature is relatively low, the rate function aligns with the results from pure states. However, at higher temperatures, the rate function becomes smooth, no longer exhibiting non-analytic critical points. This indicates that the DQPT in mixed states disappears at high temperatures. Similar to the discussion in the SSH-3 model, we can also understand the behavior of dynamic quantum phase transitions in mixed states at finite temperatures based on the behavior of

pure-state DQPTs. When the temperature is low, the probabilities of different thermodynamic states satisfy $f_{k1} \gg f_{k2} > f_{k3} > f_{k4}$, thus the generalized Loschmidt amplitude of the system is approximately equal to the Loschmidt amplitude from quenching starting from the lowest energy band in the pure state. Therefore, at low temperatures, the behavior of DQPTs is the same as that of pure states. However, at high temperatures, due to the contribution of higher energy bands that cannot be neglected and the different critical wave vectors in quenching processes starting from various bands, the generalized Loschmidt amplitude does not exhibit Fisher zeros, leading to the disappearance of DQPTs in mixed states.

VI. CONCLUSION

In this paper, we explore DQPTs for both pure and mixed states within the generalized SSH model, focusing on two representative configurations: the SSH-3 and SSH-4 models, which exhibit different symmetries. The SSH-3 model does not possess chiral symmetry; instead, it features a chiral-like symmetry known as point sym-

metry, which gives rise to robust, localized edge states linked to the system's topological properties. Our findings indicate that DQPTs for the pure state occur after a quench that crosses the topological transition, even when the energy band gap is open. In the case of mixed states, the DQPT behavior remains unaffected at low temperatures. However, significant changes in DQPT characteristics arise at high temperatures, leading to the emergence of multiple critical times within the system. Conversely, the SSH-4 model exhibits chiral symmetry and allows us to examine two distinct energy spectrum configurations. We find that the occurrence of DQPTs for the pure state requires the quench to start from an initial state without a band gap and to cross the critical point of the topological transition. For mixed states, DQPTs are absent at high temperatures.

ACKNOWLEDGMENTS

K. Cao thanks Mrs. H. Zhou and prof. P. Tong for the valuable suggestion. The work is supported by the National Natural Science Foundation of China (Grant No. 11875047).

-
- [1] I. Bloch, J. Dalibard, and W. Zwerger, Many-body physics with ultracold gases, *Rev. Mod. Phys.* **80**, 885 (2008).
 - [2] M. Lewenstein, A. Sanpera, and V. Ahufinger, *Ultracold Atoms in Optical Lattices: Simulating quantum many-body systems* (Oxford University Press, 2012).
 - [3] A. Polkovnikov, K. Sengupta, A. Silva, and M. Vengalattore, Colloquium: Nonequilibrium dynamics of closed interacting quantum systems, *Rev. Mod. Phys.* **83**, 863 (2011).
 - [4] A. Mitra, Quantum quench dynamics, *Annual Review of Condensed Matter Physics* **9**, 245 (2018).
 - [5] W. H. Zurek, U. Dorner, and P. Zoller, Dynamics of a quantum phase transition, *Phys. Rev. Lett.* **95**, 105701 (2005).
 - [6] M. Heyl, A. Polkovnikov, and S. Kehrein, Dynamical quantum phase transitions in the transverse-field ising model, *Phys. Rev. Lett.* **110**, 135704 (2013).
 - [7] A. A. Zvyagin, Dynamical quantum phase transitions (review article), *Low Temperature Physics* **42**, 971 (2016).
 - [8] M. Heyl, Dynamical quantum phase transitions: a review, *Reports on Progress in Physics* **81**, 054001 (2018).
 - [9] S. Vajna and B. Dóra, Disentangling dynamical phase transitions from equilibrium phase transitions, *Phys. Rev. B* **89**, 161105 (2014).
 - [10] U. Divakaran, S. Sharma, and A. Dutta, Tuning the presence of dynamical phase transitions in a generalized xy spin chain, *Phys. Rev. E* **93**, 052133 (2016).
 - [11] K. Cao, M. Zhong, and P. Tong, Dynamical quantum phase transition in XY chains with the dzyaloshinskii-moriya and XZY-YZX three-site interactions, *Chinese Physics B* **31**, 060505 (2022).
 - [12] S. Porta, F. Cavaliere, M. Sasseti, and N. T. Ziani, Topological classification of dynamical quantum phase transitions in the xy chain, *Scientific Reports* **10**, 10.1038/s41598-020-69621-8 (2020).
 - [13] M. Schmitt and S. Kehrein, Dynamical quantum phase transitions in the kitaev honeycomb model, *Phys. Rev. B* **92**, 075114 (2015).
 - [14] C. Karrasch and D. Schuricht, Dynamical phase transitions after quenches in nonintegrable models, *Phys. Rev. B* **87**, 195104 (2013).
 - [15] F. Andraschko and J. Sirker, Dynamical quantum phase transitions and the loschmidt echo: A transfer matrix approach, *Phys. Rev. B* **89**, 125120 (2014).
 - [16] M. Heyl, Dynamical quantum phase transitions in systems with broken-symmetry phases, *Phys. Rev. Lett.* **113**, 205701 (2014).
 - [17] J. N. Kriel, C. Karrasch, and S. Kehrein, Dynamical quantum phase transitions in the axial next-nearest-neighbor ising chain, *Phys. Rev. B* **90**, 125106 (2014).
 - [18] S. Sharma, S. Suzuki, and A. Dutta, Quenches and dynamical phase transitions in a nonintegrable quantum ising model, *Phys. Rev. B* **92**, 104306 (2015).
 - [19] J. C. Halimeh and V. Zauner-Stauber, Dynamical phase diagram of quantum spin chains with long-range interactions, *Phys. Rev. B* **96**, 134427 (2017).
 - [20] I. Homrighausen, N. O. Abeling, V. Zauner-Stauber, and J. C. Halimeh, Anomalous dynamical phase in quantum spin chains with long-range interactions, *Phys. Rev. B* **96**, 104436 (2017).
 - [21] T. Obuchi, S. Suzuki, and K. Takahashi, Complex semiclassical analysis of the loschmidt amplitude and dynamical quantum phase transitions, *Phys. Rev. B* **95**, 174305 (2017).

- [22] V. Zauner-Stauber and J. C. Halimeh, Probing the anomalous dynamical phase in long-range quantum spin chains through fisher-zero lines, *Phys. Rev. E* **96**, 062118 (2017).
- [23] A. Dutta and A. Dutta, Probing the role of long-range interactions in the dynamics of a long-range kitaev chain, *Phys. Rev. B* **96**, 125113 (2017).
- [24] B. Žunkovič, M. Heyl, M. Knap, and A. Silva, Dynamical quantum phase transitions in spin chains with long-range interactions: Merging different concepts of nonequilibrium criticality, *Phys. Rev. Lett.* **120**, 130601 (2018).
- [25] J. C. Halimeh, M. Van Damme, V. Zauner-Stauber, and L. Vanderstraeten, Quasiparticle origin of dynamical quantum phase transitions, *Phys. Rev. Res.* **2**, 033111 (2020).
- [26] C. Karrasch and D. Schuricht, Dynamical quantum phase transitions in the quantum potts chain, *Phys. Rev. B* **95**, 075143 (2017).
- [27] L. Zhou, Q.-h. Wang, H. Wang, and J. Gong, Dynamical quantum phase transitions in non-hermitian lattices, *Phys. Rev. A* **98**, 022129 (2018).
- [28] D. Mondal and T. Nag, Anomaly in the dynamical quantum phase transition in a non-hermitian system with extended gapless phases, *Phys. Rev. B* **106**, 054308 (2022).
- [29] D. Mondal and T. Nag, Finite-temperature dynamical quantum phase transition in a non-hermitian system, *Phys. Rev. B* **107**, 184311 (2023).
- [30] L.-J. Zhai, G.-Y. Huang, and S. Yin, Nonequilibrium dynamics of the localization-delocalization transition in the non-hermitian aubry-andré model, *Phys. Rev. B* **106**, 014204 (2022).
- [31] M. Abdi, Dynamical quantum phase transition in bose-einstein condensates, *Phys. Rev. B* **100**, 184310 (2019).
- [32] K. Yang, L. Zhou, W. Ma, X. Kong, P. Wang, X. Qin, X. Rong, Y. Wang, F. Shi, J. Gong, and J. Du, Floquet dynamical quantum phase transitions, *Phys. Rev. B* **100**, 085308 (2019).
- [33] S. Zamani, R. Jafari, and A. Langari, Floquet dynamical quantum phase transition in the extended xy model: Nonadiabatic to adiabatic topological transition, *Phys. Rev. B* **102**, 144306 (2020).
- [34] T. Shirai, S. Todo, and S. Miyashita, Dynamical phase transition in floquet optical bistable systems: An approach from finite-size quantum systems, *Phys. Rev. A* **101**, 013809 (2020).
- [35] L. Zhou and Q. Du, Floquet dynamical quantum phase transitions in periodically quenched systems, *Journal of Physics: Condensed Matter* **33**, 345403 (2021).
- [36] R. Jafari and A. Akbari, Floquet dynamical phase transition and entanglement spectrum, *Phys. Rev. A* **103**, 012204 (2021).
- [37] R. Hamazaki, Exceptional dynamical quantum phase transitions in periodically driven systems, *Nature Communications* **12**, 5108 (2021).
- [38] S. Zamani, R. Jafari, and A. Langari, Out-of-time-order correlations and floquet dynamical quantum phase transition, *Phys. Rev. B* **105**, 094304 (2022).
- [39] R. Jafari, A. Akbari, U. Mishra, and H. Johannesson, Floquet dynamical quantum phase transitions under synchronized periodic driving, *Phys. Rev. B* **105**, 094311 (2022).
- [40] U. Bhattacharya, S. Bandyopadhyay, and A. Dutta, Mixed state dynamical quantum phase transitions, *Phys. Rev. B* **96**, 180303 (2017).
- [41] M. Heyl and J. C. Budich, Dynamical topological quantum phase transitions for mixed states, *Phys. Rev. B* **96**, 180304 (2017).
- [42] H. Lang, Y. Chen, Q. Hong, and H. Fan, Dynamical quantum phase transition for mixed states in open systems, *Phys. Rev. B* **98**, 134310 (2018).
- [43] S. Bandyopadhyay, S. Laha, U. Bhattacharya, and A. Dutta, Exploring the possibilities of dynamical quantum phase transitions in the presence of a markovian bath, *Scientific Reports* **8**, 10.1038/s41598-018-30377-x (2018).
- [44] X.-Y. Hou, Q.-C. Gao, H. Guo, Y. He, T. Liu, and C.-C. Chien, Ubiquity of zeros of the loschmidt amplitude for mixed states in different physical processes and its implication, *Phys. Rev. B* **102**, 104305 (2020).
- [45] T. H. Kyaw, V. M. Bastidas, J. Tangpanitanon, G. Romero, and L.-C. Kwek, Dynamical quantum phase transitions and non-markovian dynamics, *Phys. Rev. A* **101**, 012111 (2020).
- [46] B. Mera, C. Vlachou, N. Paunković, V. R. Vieira, and O. Viyuela, Dynamical phase transitions at finite temperature from fidelity and interferometric loschmidt echo induced metrics, *Phys. Rev. B* **97**, 094110 (2018).
- [47] N. Sedlmayr, M. Fleischhauer, and J. Sirker, Fate of dynamical phase transitions at finite temperatures and in open systems, *Phys. Rev. B* **97**, 045147 (2018).
- [48] V. Link and W. T. Strunz, Dynamical phase transitions in dissipative quantum dynamics with quantum optical realization, *Phys. Rev. Lett.* **125**, 143602 (2020).
- [49] X.-Y. Hou, H. Guo, and C.-C. Chien, Finite-temperature topological phase transitions of spin- j systems in uhlmann processes: General formalism and experimental protocols, *Phys. Rev. A* **104**, 023303 (2021).
- [50] N. Fläschner, D. Vogel, M. Tarnowski, B. S. Rem, D. S. Lühmann, M. Heyl, J. C. Budich, L. Mathey, K. Sengstock, and C. Weitenberg, Observation of dynamical vortices after quenches in a system with topology, *Nature Physics* **14**, 265 (2017).
- [51] P. Jurcevic, H. Shen, P. Hauke, C. Maier, T. Brydges, C. Hempel, B. P. Lanyon, M. Heyl, R. Blatt, and C. F. Roos, Direct observation of dynamical quantum phase transitions in an interacting many-body system, *Phys. Rev. Lett.* **119**, 080501 (2017).
- [52] Z. Chen, J.-M. Cui, M.-Z. Ai, R. He, Y.-F. Huang, Y.-J. Han, C.-F. Li, and G.-C. Guo, Experimentally detecting dynamical quantum phase transitions in a slowly quenched ising-chain model, *Phys. Rev. A* **102**, 042222 (2020).
- [53] J. A. Muniz, D. Barberena, R. J. Lewis-Swan, D. J. Young, J. R. K. Cline, A. M. Rey, and J. K. Thompson, Exploring dynamical phase transitions with cold atoms in an optical cavity, *Nature* **580**, 602 (2020).
- [54] X. Nie, B.-B. Wei, X. Chen, Z. Zhang, X. Zhao, C. Qiu, Y. Tian, Y. Ji, T. Xin, D. Lu, and J. Li, Experimental observation of equilibrium and dynamical quantum phase transitions via out-of-time-ordered correlators, *Phys. Rev. Lett.* **124**, 250601 (2020).
- [55] K. Wang, X. Qiu, L. Xiao, X. Zhan, Z. Bian, W. Yi, and P. Xue, Simulating dynamic quantum phase transitions in photonic quantum walks, *Phys. Rev. Lett.* **122**, 020501 (2019).
- [56] X. Y. Xu, Q. Q. Wang, M. Heyl, J. C. Budich, W. W. Pan, Z. Chen, M. Jan, K. Sun, J. S. Xu, Y. J. Han, C. F. Li, and G. C. Guo, Measuring a dynamical topological

- order parameter in quantum walks, *Light-Science Applications* **9**, 10.1038/s41377-019-0237-8 (2020).
- [57] T. Tian, H.-X. Yang, L.-Y. Qiu, H.-Y. Liang, Y.-B. Yang, Y. Xu, and L.-M. Duan, Observation of dynamical quantum phase transitions with correspondence in an excited state phase diagram, *Phys. Rev. Lett.* **124**, 043001 (2020).
- [58] E. A. Yuzbashyan, O. Tsypliyatyev, and B. L. Altshuler, Relaxation and persistent oscillations of the order parameter in fermionic condensates, *Phys. Rev. Lett.* **96**, 097005 (2006).
- [59] P. Barmettler, M. Punk, V. Gritsev, E. Demler, and E. Altman, Relaxation of antiferromagnetic order in spin-1/2 chains following a quantum quench, *Phys. Rev. Lett.* **102**, 130603 (2009).
- [60] M. Eckstein, M. Kollar, and P. Werner, Thermalization after an interaction quench in the hubbard model, *Phys. Rev. Lett.* **103**, 056403 (2009).
- [61] B. Sciolla and G. Biroli, Quantum quenches and off-equilibrium dynamical transition in the infinite-dimensional bose-hubbard model, *Phys. Rev. Lett.* **105**, 220401 (2010).
- [62] J. Dziarmaga, Dynamics of a quantum phase transition and relaxation to a steady state, *Advances in Physics* **59**, 1063 (2010).
- [63] J. C. Budich and M. Heyl, Dynamical topological order parameters far from equilibrium, *Phys. Rev. B* **93**, 085416 (2016).
- [64] S. Vajna and B. Dóra, Topological classification of dynamical phase transitions, *Phys. Rev. B* **91**, 155127 (2015).
- [65] Z. Huang and A. V. Balatsky, Dynamical quantum phase transitions: Role of topological nodes in wave function overlaps, *Phys. Rev. Lett.* **117**, 086802 (2016).
- [66] K. Cao, H. Guo, and G. Yang, Aperiodic dynamical quantum phase transition in multi-band bloch hamiltonian and its origin, *Journal of Physics: Condensed Matter* **36**, 155401 (2024).
- [67] A. Anastasiadis, G. Styliaris, R. Chaunsali, G. Theocharis, and F. K. Diakonov, Bulk-edge correspondence in the trimer su-schrieffer-heeger model, *Phys. Rev. B* **106**, 085109 (2022).
- [68] C.-S. Lee, I.-F. Io, and H. chung Kao, Winding number and zak phase in multi-band ssh models, *Chinese Journal of Physics* **78**, 96 (2022).
- [69] E. Sjöqvist, A. K. Pati, A. Ekert, J. S. Anandan, M. Ericsson, D. K. L. Oi, and V. Vedral, Geometric phases for mixed states in interferometry, *Phys. Rev. Lett.* **85**, 2845 (2000).
- [70] D. M. Tong, E. Sjöqvist, L. C. Kwek, and C. H. Oh, Kinematic approach to the mixed state geometric phase in nonunitary evolution, *Phys. Rev. Lett.* **93**, 080405 (2004).
- [71] J.-C. Tang, X.-Y. Hou, and H. Guo, Parallel quench and dynamic geometrical order parameter (2024), arXiv:2410.17940 [quant-ph].
- [72] Y. He and C.-C. Chien, Non-hermitian generalizations of extended su-schrieffer-heeger models, *Journal of Physics: Condensed Matter* **33**, 085501 (2020).